1   **Influence of Nb and Ta on the Corrosion and Mechanical Properties of CrYN Coatings**

2   Banu Yaylali[1], Gokhan Gulten[1], Ihsan Efeoglu[1*], Yasar Totik[1], Peter Kelly[2] and Justyna

3   Kulczyk-Malecka[2]

4   [1]Faculty of Engineering, Department of Mechanical Engineering, Atatürk University, 25240 Erzurum, Türkiye

5   [2] Surface Engineering Group, Manchester Metropolitan University, Manchester M1 5GD, UK

6   *Corresponding author.

7   E-mail address: iefeoğlu@atauni.edu.tr (İhsan Efeoğlu)

8

9   **Abstract**

10   Barrier coatings are applied to many machine components that are exposed to aggressive/harsh

11   service conditions to prevent corrosion, oxidation, and wear at high temperatures. These

12   coatings are widely used to protect structural components of gas/steam turbines in the energy

13   and aerospace industries against aggressive operating conditions. In this study, Nb and Ta-

14   doped CrYN films were deposited onto 316L stainless steel (SS) using the CFUBMS (Closed

15   Field Unbalanced Magnetron Sputtering) technique. Then, the corrosion resistance, and

16   structural and mechanical properties of the CrYN:Nb/Ta thin films were investigated. SEM,

17   XPS, EDS, nanoindentation and potentiostat tester were used to determine the structural,

18   mechanical and corrosion properties of the thin films, respectively. The highest hardness was

19   found to be 21.4 GPa for CrYN:Nb films and 18.2 GPa for CrYN: Ta films. The results show

20   that the coated specimens (lowest Icorr value 3.7 nA obtained in all tests) have higher corrosion

21   resistance than the uncoated specimens (substrate Icorr value 1826 nA). In addition, it has been

22   observed that the corrosion resistance of Ta-doped CrYN thin films is somewhat better than the

23   niobium-doped thin films.

24   **Keywords:** CrYN:Nb/Ta thin films, PVD, Pulsed-Dc, Corrosion

25   **1. Introduction**

26   Thermal barrier coatings (TBC) are used to protect component(s) and increase service life in

27   high-temperature applications such as gas/steam turbines, jet engines/blades, and fuel cells.

28   TBCs are expected to withstand high temperature, high pressure, temperature differences, wear,

29   complex stress conditions, and corrosion [1]. However, there is no simple coating system that

30   can meet all these parameters on its own. This has led researchers to produce more complex

coating architectural systems [2, 3]. For this reason, complex thermal barrier coatings consisting of four main components, each with different mechanical, tribological, and chemical properties, have been developed [4]. The first of these components is the metallic substrate made of stainless steel or super alloys, which carries the mechanical load [5]. Second; the bond layer that increases the adhesion and bond strength with the top layer, consisting of MCrAlY (M=Ni, Co), reduces the stress at the interface by minimising the thermal expansion differences between the metallic substrate and the ceramic top layer and protects different types of metallic substrates against oxidation and corrosion as a diffusion barrier. [1, 2, 4, 6-9]. The ideal bond coat is commonly described in the literature with this structure to ensure that the formation and growth of thermally grown oxide as Al_2O_3 is slow, uniform and defect-free [1, 10]. Third; Thermally grown oxide (TGO) layer is formed as a result of oxygen and aluminum diffusion at the interface between the ceramic top layer and the bond layer as a result of thermal cycles during operating conditions under the influence of high temperature. TGO formation is inevitable [1, 10, 11]. The thickness of this layer increases due to oxygen diffusing continuously from the ceramic layer and aluminum diffusing from the bond layer. Although the thickness of the TGO layer varies in the range of 1-10 μm, a thickness of 6 μm and above is undesirable because it reduces the thermal cycle life of the coating [1, 2]. Studies are being carried out to control this structure [11]. The last of the TBC components is the ceramic layer that forms the top layer of the thermal barrier coating system. This layer protects the metallic substrate against heat by acting as thermal insulation. For this reason, it is defined as the most important part of the system. Desired properties of the ceramic top layer can be summarized as low thermal conductivity, high melting temperature, thermal expansion compatibility (metallic base/metallic bond coat), resistance to phase transformation (from room temperature to service conditions), good adhesion, high resistance to corrosion, erosion, and oxidation [1, 2, 12]. The industry's most preferred ceramic top layer is zirconia stabilized with yttrium, produced by a plasma spray method. However, phase transformation occurs in YSZ (YSZ: yttria-stabilized zirconia) at temperatures of 1170 °C and above, resulting in separation, delamination, and damage to the coating [1, 2, 13].

As a result of day by day developing technology, gas/steam turbines, aircraft/jet engines and high temperature components are required to operate under supercritical conditions with minimal losses [14-16]. This continuously encourages researchers to synthesize alternative barrier coatings. The aim of the research is to synthesize thin films that can be an alternative to thermal barrier coatings resistant to high temperature, high pressure, abrasion, corrosion and oxidation for use in high temperature applications such as jet/aircraft engines, fuel cells,

gas/steam turbines. A number of studies show that chromium nitride, chromium yttrium nitride and chromium aluminum nitride coatings may be suitable for high temperature and high pressure applications [15, 17-19, 20-22]. CrN coatings have a fine-grained structure, low internal stress, high hardness and corrosion resistance [23]. CrN films are known to have better corrosion resistance, high hardness and thermal stability even at high temperatures (up to 700 °C) than TiN thin films [19, 23-27]. Researchers are trying to improve the structural, chemical and tribological properties by adding elements such as aluminum, yttrium, molybdenum, niobium, tantalum, etc. to the structure that is inadequate at high temperatures [15, 17, 19, 20-22, 28]. In a paper by Hovsepian et al., the structure's superior wear and corrosion resistance was attributed to high hardness Me-nitrides of relatively electrochemically inert elements such as Cr and Nb [15]. It is well known that oxidation resistance and thermal stability can be improved by adding yttrium to protective coatings used at high temperatures [25, 30]. In the literature, it has been reported that by adding Nb (Niobium) to nitride-based coatings, solid solution formation can be increased, a finer-grained, dense, and homogenous microstructure can be obtained, thus improving mechanical properties and showing a positive trend for corrosion resistance [15, 28-31]. The positive effects of tantalum (Ta) additives on corrosion resistance are already known [28, 32]. Due to their chemical stability in corrosive environments, CrN films show high resistance to corrosion in Cl^- solution. The Cr_2N phase is more resistant to corrosion than the chromium nitride phase. Bertrand et al. observed in a study that the intrinsic behavior of Cr_2N is better than that of CrN in acidic or chloride solutions. It is thought that corrosion resistance increases in direct proportion to the presence and amount of Cr_2N phase in the structure [33-36]. In addition, nitride-based films tend to form thin and hard films due to both their nature and manufacturing methods.

In this study hard thin films were deposited by adding Nb and Ta to CrYN films. The synthesis process was carried out by closed-field unbalanced magnetron sputtering (CFUBMS) and 316 L stainless steel was used as the substrate.

2. Materials and Methods

316L stainless steel (SS) material was preferred as the substrate for synthesized CrYN:Nb/Ta films. The substrates were polished from coarse to fine grain with 400, 600, 800, 1000, and 1200 mesh SiC abrasives, respectively, and the surface roughness was brought to Ra≈0.02 μm. Before the process, they were washed with acetone + ethyl alcohol in an ultrasonic bath (30 min.) to increase the adhesion to the coating and to passivate the surface. The substrates were

1 then etched in a solution of V2A Etchant (100 ml distilled water, 100 ml HCl and 10 ml nitric

2 acid).

3 Two (99.95%) CrY targets (atomic percent Cr 97%, Y 3%), one (99.95%) niobium or one

4 (99.95%) tantalum target were used to synthesize CrYN:Nb/Ta film in the process. The coating

5 process was performed using the CFUBMS (Closed Field Unbalanced Magnetron Sputtering)

6 technique, operating in DC or pulsed DC mode. N_2 gas was used as the reactive gas (99.99%),

7 and Ar gas (99.99%) was used for plasma formation and sputtering of the targets. In order to

8 increase the adhesion between the substrate and the coating and to remove contaminants from

9 the substrate, cleaning was performed with Ar+ ions for 30 minutes at -800 V bias voltage just

10 before the deposition process. Then, in order to increase the adhesion, a CrY interlayer was

11 deposited for 10 minutes at 2A target power. A Taguchi L9 orthogonal design was used to

12 design the coating process experiments; all coating parameters are detailed in Table 1. The

13 deposition parameters investigated in the array were target current (1, 1.5, and 2 A), deposition

14 pressure (0.15, 0.25, and 0.35 Pa), pulse frequency (100, 200, and 350 kHz), and duty cycle

15 (50-70-85 %). Pulsed-Dc (CrY target) and Dc power (Nb and Ta target) supplies were used in

16 the synthesis process. The architecture of the stored microstructure and a representation of the

17 Teer Coating Ltd. patented CFUBMS system are both shown schematically in Figure 1.

18
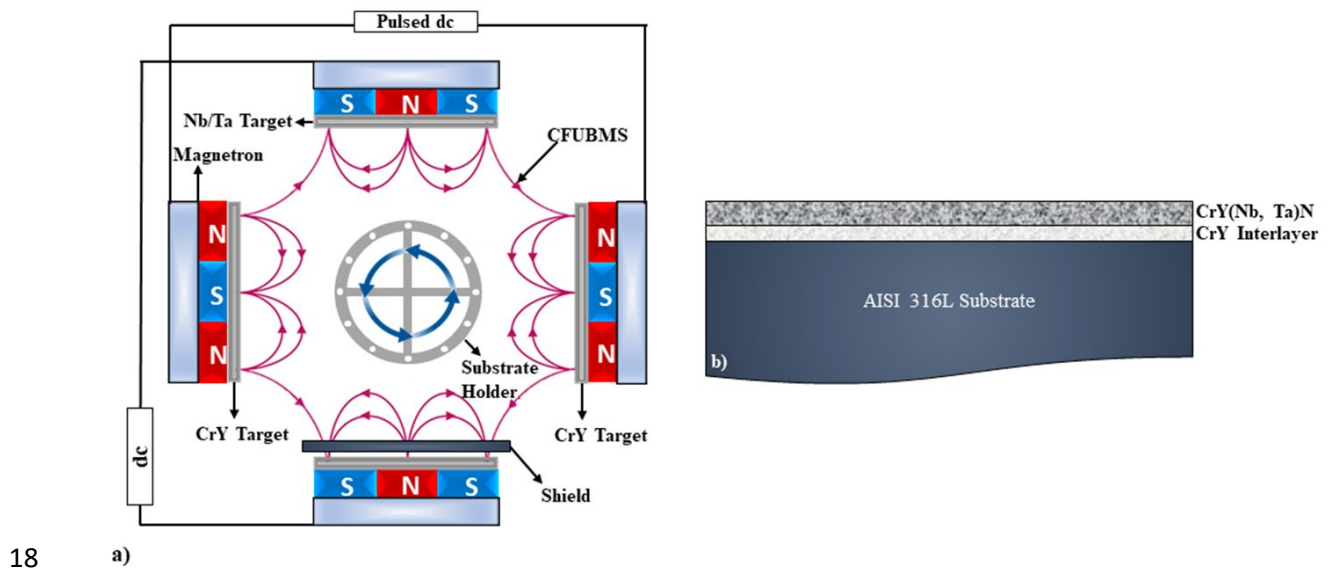
19 **Fig. 1. a)** Magnetron sputtering system and **b)** Architectural structure of CrYN:Nb/Ta thin films

20 **Table 1.** Deposition Parameters and Taguchi Experimental Design [37]

The variable Parameters	Level 1	Level 2	Level 3
CrY Target Current (A)	1	1.5	2
Deposition Pressure (Pa)	0.15	0.25	0.35
Pulse Frequency (kHz)	100	200	350
Duty Cycle (%)	50	70	85

The Constant Parameters	
CrY Interlayer	CrY: 2A (10 min)
CrY (Nb, Ta)N	Nb: 2A, Ta: 2A (90 min)
N_2 Flow Rate (sccm)	6
Substrate Bias (-V)	50

|	Pulse Frequency (kHz)	Duty Cycle (%)	Deposition Pressure (Pa)	CrY Target Current (A)
R1	100	50	0.15	1
R2	100	70	0.25	1.5
R3	100	85	0.35	2
R4	200	50	0.25	2
R5	200	70	0.35	1
R6	200	85	0.15	1.5
R7	350	50	0.35	1.5
R8	350	70	0.25	2
R9	350	85	0.15	1

The nanohardness analysis of the thin films was performed using a nanoindentation tester manufactured by Anton Paar. Maximum load: 3.00 mN, Loading rate: 6.00 mN/min was applied for 10 seconds using a Berkovich indenter. X-ray diffraction (XRD) was performed with a Cu-Kα radiation source in a Rigaku 2000 D max diffractometer over the range of 20° and 90° 2 theta and 2°/min scan rate. A Zeiss Sigma 300 scanning electron microscope (SEM) was used for examination of the microstructure and surface morphology of the coatings, and a XPS (X-Ray Photoelectron Spectroscopy) and energy dispersive spectroscopy (EDS) device was used for elemental analysis. Electrochemical polarization experiments for corrosion were carried out using a computer-controlled Versastat3 Potentiostat device. Three-electrode cell configurations were preferred for polarization measurements. Corrosion tests were performed in 3.5% NaCl solution. The electrochemical cell consists of a working electrode (WE), a standard Ag/AgCl reference electrode (RE) and a graphite counter electrode (CE), and coated CrYN:Nb/Ta samples. The scanning rate was determined as 0.5 mV/s in the corrosion experiments. After the corrosion tests, the surface images of the samples showing the best and worst corrosion potential according to the results were examined by SEM (FEI Quanta FEG-450 SEM-EDS), followed by EDS analysis.

3. Results and discussions

XPS was used to determine the chemical composition of the CrYN:Nb/Ta thin films. XPS provides information about the chemical states and binding energies of the elements in the

resulting structure, and the resulting spectra indicate the binding energies of photoelectrons. Shifts in binding energies indicate changes in the physical and chemical properties of the structure. The cumulative curves of the XPS spectra of chromium (Cr2p), yttrium (Y3d), nitrogen (N1s) and niobium (Nb3d) for the CrYN:Nb thin films are plotted using the Gaussian method and given in Figure 2. $Cr2p_{3/2}$, $Y3d_{5/2}$, $Nb3d_{5/2}$ and N1s peaks can be observed in the graphs (Figure 2). The binding energies of the peaks were determined as 570 ± 2, 150 ± 6, 200 ± 3 and 393 ± 3 eV, respectively
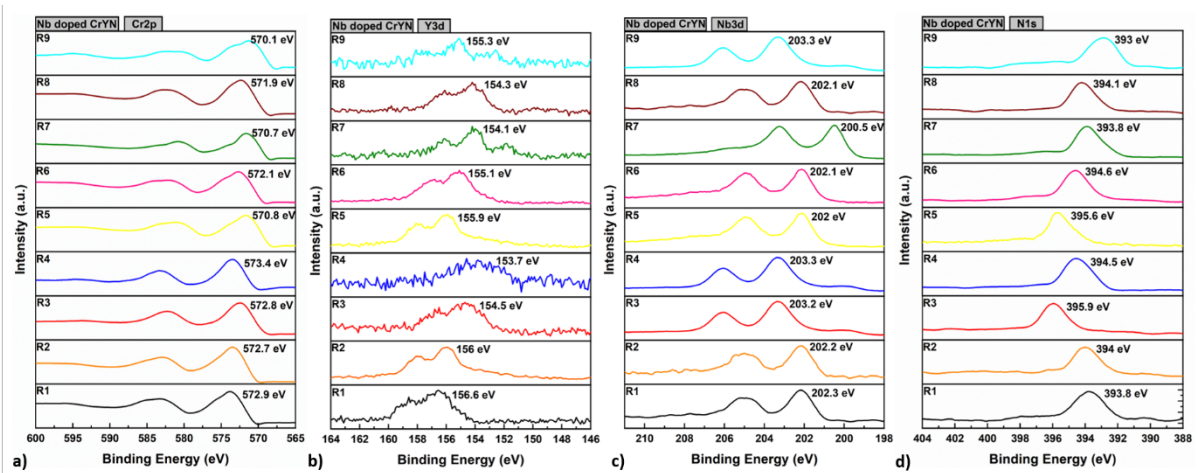
Fig. 2. CrYN:Nb thin films, a) Chromium (Cr2p), b) Yttrium (Y3d), c) Niobium (Nb3d), d) Nitrogen (Nb1s) XPS spectra

XPS analysis was performed for all experiments from R1 to R9 for the CrYN:Ta films. XPS spectra of chromium (Cr2p), yttrium (Y3d), nitrogen (N1s) and tantalum (Ta4d) are given in Figure 3.
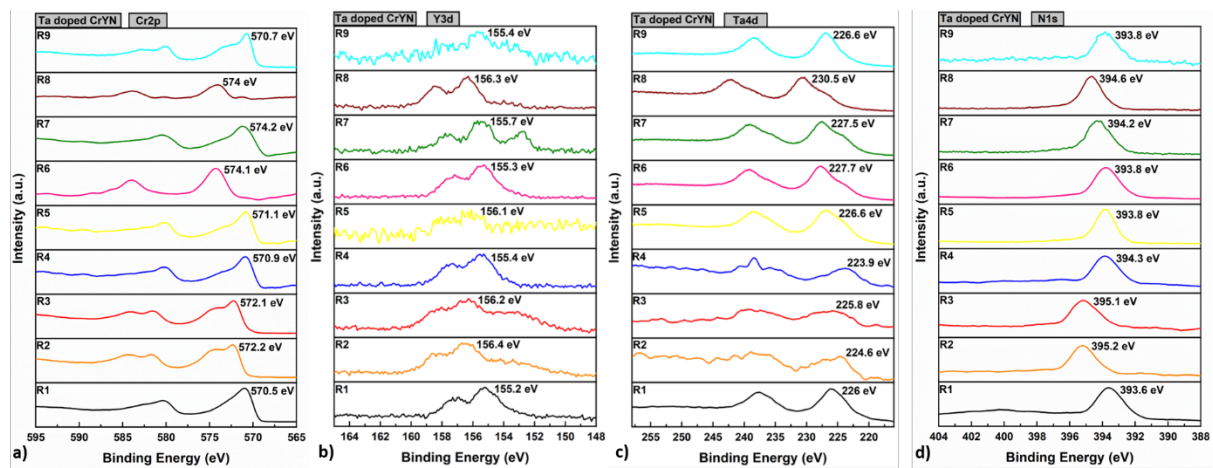
Fig. 3. CrYN:Ta thin films, a) Chromium (Cr2p), b) Yttrium (Y3d), c) Tantalum (Ta4d), d) Nitrogen (N1s) XPS spectra

When CrYN:Ta thin films were examined, $Ta4d_{5/2}$ peaks were found and observed to have a binding energy of 220 ± 7 eV (Figure 3c). Similar results were obtained for Cr, Y, and N in

CrYN:Nb thin films. When the Cr, Y, Nb, Ta and N peaks were analyzed, it was observed that some of them had significant shifts in their binding energies. The details that Cr2p and N1s binding energies decrease with the increase in nitrogen content is available in the literature [38, 39, 40]. These bonds present in our research could indicate CrN, Cr_2N, NbN or TaN.

When the nanohardness values of niobium and tantalum doped CrYN films were investigated, it was observed that the highest hardness values were 21.4 GPa and 18.2 GPa, respectively. Typical nanoindentation load-depth curves and nanohardness results for CrYN:Nb/Ta thin films are given in Figure 4.

Table 2. Elemental composition of Nb doped CrYN thin films

		R1	R2	R3	R4	R5	R6	R7	R8	R9
	Cr	44.09	34.64	73.33	56.21	41.54	57.97	39.9	55.29	31.25
at. %	**Y**	0.99	1.21	1.56	0.93	0.88	1.03	0.75	0.76	0.61
	N	38.39	34.64	20.39	29.67	42.37	29.33	43.28	28.91	50.32
	Nb	16.54	10.63	4.73	13.19	15.22	11.67	16.06	15.04	17.82

Table 3. Elemental composition of Ta doped CrYN thin films

		R1	R2	R3	R4	R5	R6	R7	R8	R9
	Cr	29.2	50.94	61.04	52.31	34.3	52.95	41.59	49.03	29.5
at. %	**Y**	1.47	1.36	1.56	1.16	1.42	1.3	1.15	1.42	1.55
	N	42.68	30.56	24.5	25.92	37.97	27.05	30.67	28.81	38.28
	Ta	26.65	17.13	12.9	20.61	26.32	18.71	26.59	20.74	30.68

EDS results of CrYN:Nb/Ta thin films are given in Tables 3 and 4. When the experimental parameters are examined, the highest Cr and Y amounts were obtained in experiments R3, R4 and R8 with the highest target current. The percentage contents of the targets used in the material and method are stated as 97% Cr and 3% Y. The yttrium content of 0.5-1.6% in the coating content can be attributed to the low yttrium content in the target. Based on the knowledge that the working pressure and N_2/Ar ratio are inversely related, it can be said that the increase in nitrogen content is related to the decrease in pressure.
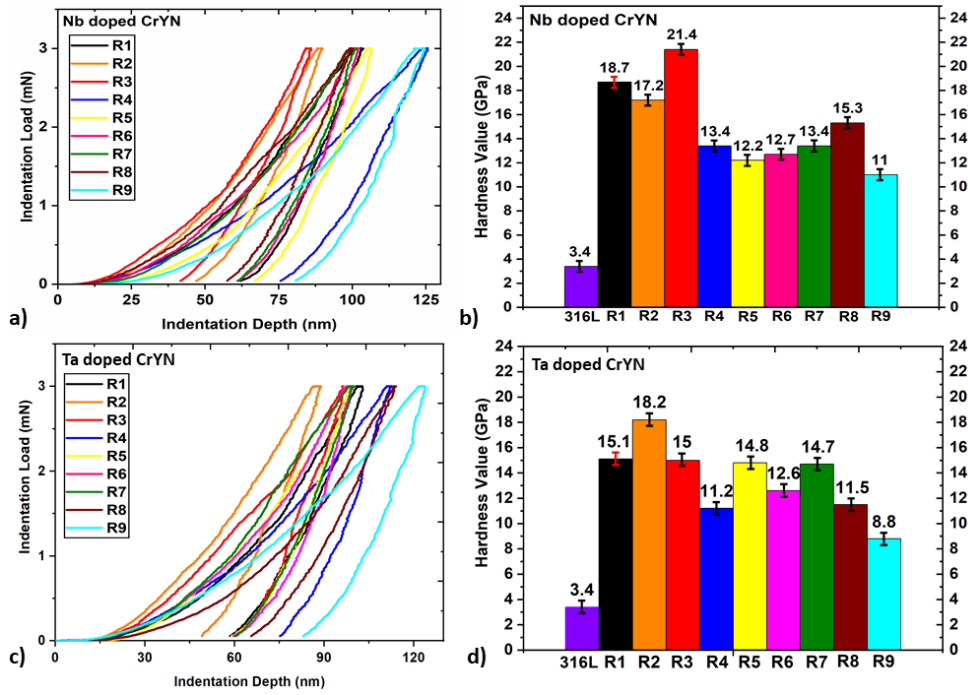
Fig. 4. a-c) Typical nanoindentation load-depth curves for CrYN:Nb/Ta thin films, **b-d)** Nanohardness values for CrYN:Nb/Ta thin films

When all experimental parameters are examined for both niobium and tantalum doped thin films, the highest hardness values are observed in R3 (CrY(Nb)N:21.4±0.5 GPa) and R2 (CrY(Ta)N: 18.2±0.5 GPa).

In a study by Wu et al., Y was added to CrN films and as a result, it was observed that the hardness of the coatings increased. It is stated in the study that this improvement can be attributed to the solid solution effect [23]. In Figure 5, H^3/E^2 and H/E values are calculated based on the hardness and elastic modulus values of all samples and the relationship between the two is given in the graph. The H/E ratio for niobium doped films ranged from 0.03 to 0.10, while for tantalum doped films this value was observed between 0.03 and 0.08. The H^3/E^2 distribution ranges from 0.02 to 0.11 and 0.01 to 0.09, respectively. In recent studies in the literature (last 10 years or so), H/E and H^3/E^2 ratios have been used to comment on fracture toughness [41, 42]. Blazek et al. reported the existence of a positive correlation between H/E (and H^3/E^2) and fracture toughness [43].
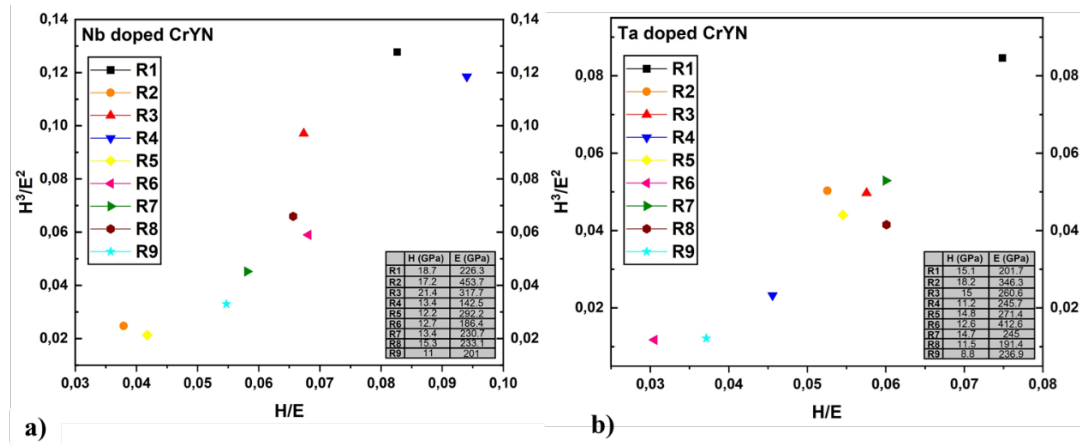
Fig. 5. Relationship between H^3/E^2 and H/E for **a)** Nb doped CrYN thin films and **b)** Ta doped thin films

When level averages are analyzed, it is observed that pulse frequency is the most significant parameter affecting this result for both dopants (Fig. 6). It is known that the addition of Nb (Niobium) to nitride-based coatings can increase solid solution formation, obtain a finer grained dense microstructure and thus improve mechanical properties [29, 31, 44]. Similarly, there is information in the literature that hardness and Young's modulus increase with increasing tantalum content in nitride-based films [45, 46].
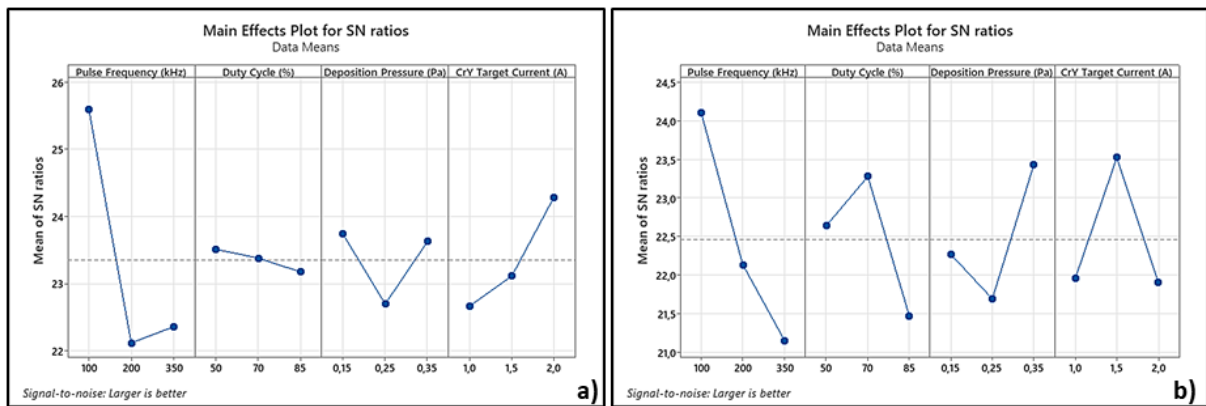

Fig. 6. Deposition parameters for nano-hardness testing of CrYN coatings level averages; **a)** Nb doped films, **b)** Ta doped films
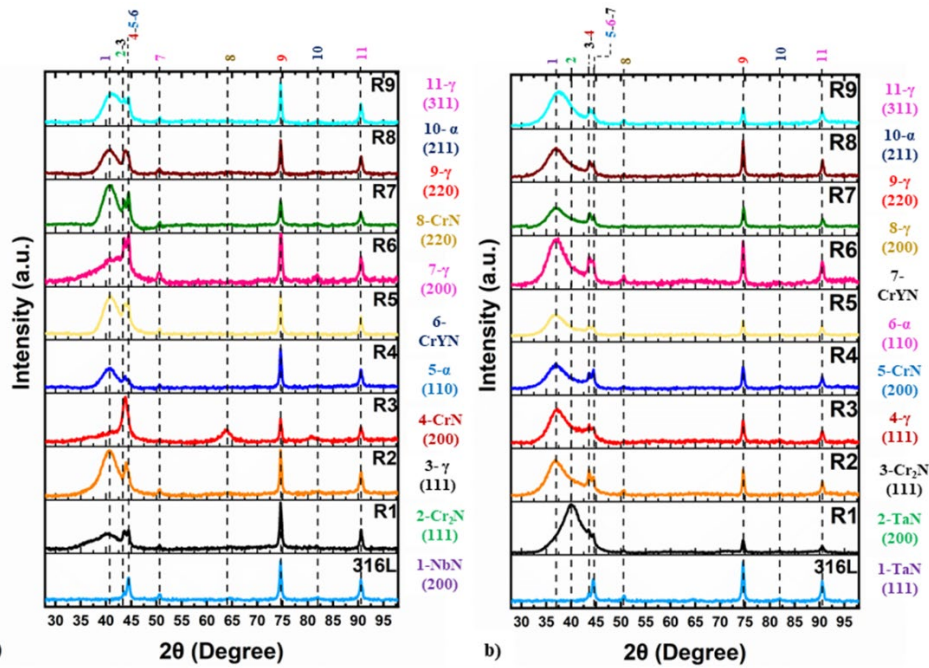
Fig. 7. XRD graph of CrYN thin films; **a)** Nb-doped and **b)** Ta-doped

XRD analysis of the Nb/Ta doped thin films deposited onto 316L stainless steel using the different array variables are presented in Figure 6. When the thin films are examined, apart from the main peaks coming from the substrate, intensely cubic CrN and Cr_2N peaks are observed. In the niobium-doped thin film, NbN and Ta-doped TaN peaks are observed (Fig. 7a and 7b), respectively. It is known from the literature that the (111) orientation seen in nitride films containing transition metals is effective on the hardness of the structure [47]. In addition, it is thought in the literature that yttrium is present in the crystal structure as a substitution atom of chromium, in this context, when XRD peaks are analyzed, it is indicated that yttrium is present in the structure as a substituent atom of chromium [48-50]. Both chromium and yttrium have 3 valence electrons. A shift of angles to the right was observed in the peak with Cr_2N phase (Fig. 6). This shift can be attributed to the fact that yttrium, which has a large atomic radius, expands the chromium cages [50].
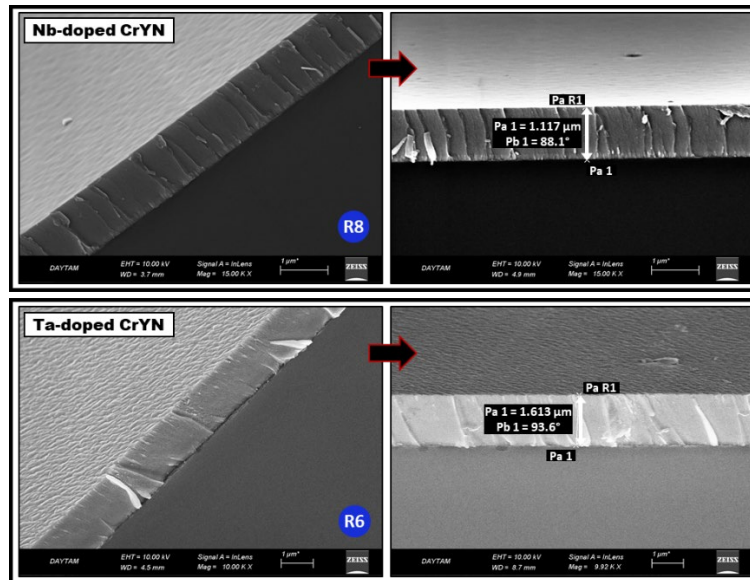
**Fig. 8.** Typical cross-sectional SEM micrographs of Nb-doped (R8) and Ta-doped (R6) CrYN thin films

Cross-sectional micrographs of films grown on Si (111) substrates were used to investigate the thickness and surface morphology properties of the nitride-based coatings (Figure 8) and, as can be seen, dense and homogeneous structures were observed in both cases. It is found that the CrY interlayer is approximately 100 nm. The highest thickness value for the niobium doped films was 2.80 µm, obtained for R3 with and the lowest thickness was obtained for R7 at 0.72 µm (Table 4). Similar results were obtained for tantalum deposited films. For CrYN:Ta films, the highest thickness value was observed in R3 with 2.26 µm and the lowest coating thickness was observed in R9 (0.99 µm).

Table 4. CrYN:Nb/Ta film thickness values

	Thickness (µm)	
Process No	Nb-CrYN (µm)	Ta-CrYN (µm)
R1	1.32	1.51
R2	1.20	1.83
R3	2.80	2.26
R4	1.33	1.73
R5	0.76	1.11
R6	1.19	1.61
R7	0.72	1.04
R8	1.11	1.23
R9	0.95	0.99

Level averages are given to comment on the most influential of the parameters. It was observed that the most effective variable for the thickness of niobium and tantalum doped chromium yttrium nitride films was pulse frequency and the weakest variable was deposition pressure (Fig. 9). Increasing target atoms sputtered with increasing CrY target current increases the deposition rate [51-53]. The highest thickness values of the CrYN:Nb/Ta films were achieved

under R3 experimental conditions at the highest current value of 2A. It is known that increasing the pulse frequency decreases the deposition rate [54]. The highest thickness and hardness values were obtained at the lowest pulse frequency for both films. Also, the R3 conditions included the highest duty factor of 85%, meaning the target was sputtered for the greatest proportion of the full pulse cycle for the conditions tested. All these parameters would be expected to promote higher deposition rates, compared to the other array conditions. In addition to all these, it is known in the literature that yttrium and niobium doping of CrN films will make the microstructure denser [48].
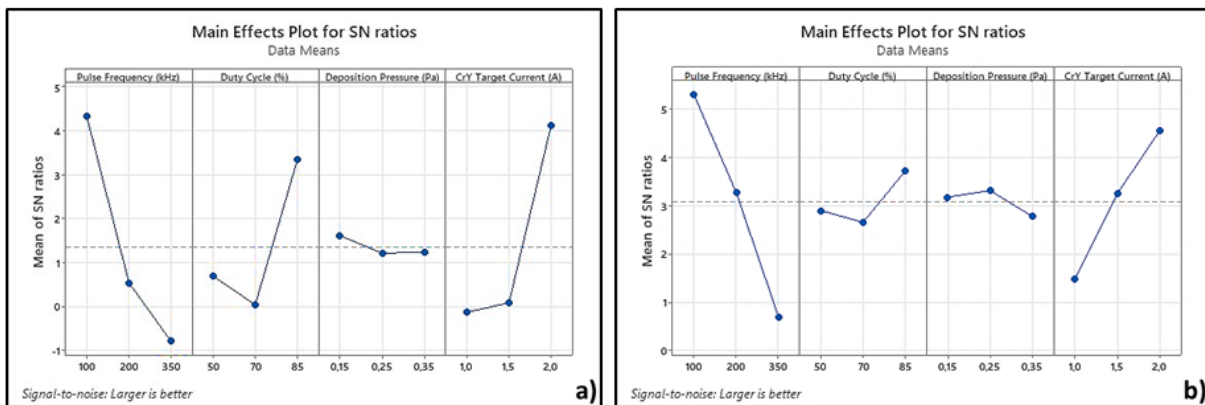
Fig. 9. Deposition parameters for film thickness of CrYN coatings level averages; **a)** Nb doped films, **b)** Ta doped films

Corrosion is a surface phenomenon and the corrosion properties of coatings on materials are mainly affected by coating thickness, phase composition and surface morphological properties (pores and cracks). The thickness and morphology of coatings appear to play a crucial role in the corrosion resistance of coated substrates. In general, coatings with low porosity and higher thickness provide better corrosion resistance. Corrosion tests for CrYN:Nb/Ta thin films were carried out in 3.5% saline solution. Potentiodynamic polarization curves of 316L substrate, niobium and tantalum doped thin films are given in Figures 10 and 11. Similar potentiodynamics polarization curves were obtained for both niobium and tantalum doped films. Ecorr and Icorr values were calculated for all samples using the Tafel analysis method. Ecorr and Icorr values are given in detail in table 3. When the Tafel curve of the substrate is analyzed, the presence of a transpassive region is observed. In addition, there is a very small transpassive region in R1 of the Nb-doped thin film.
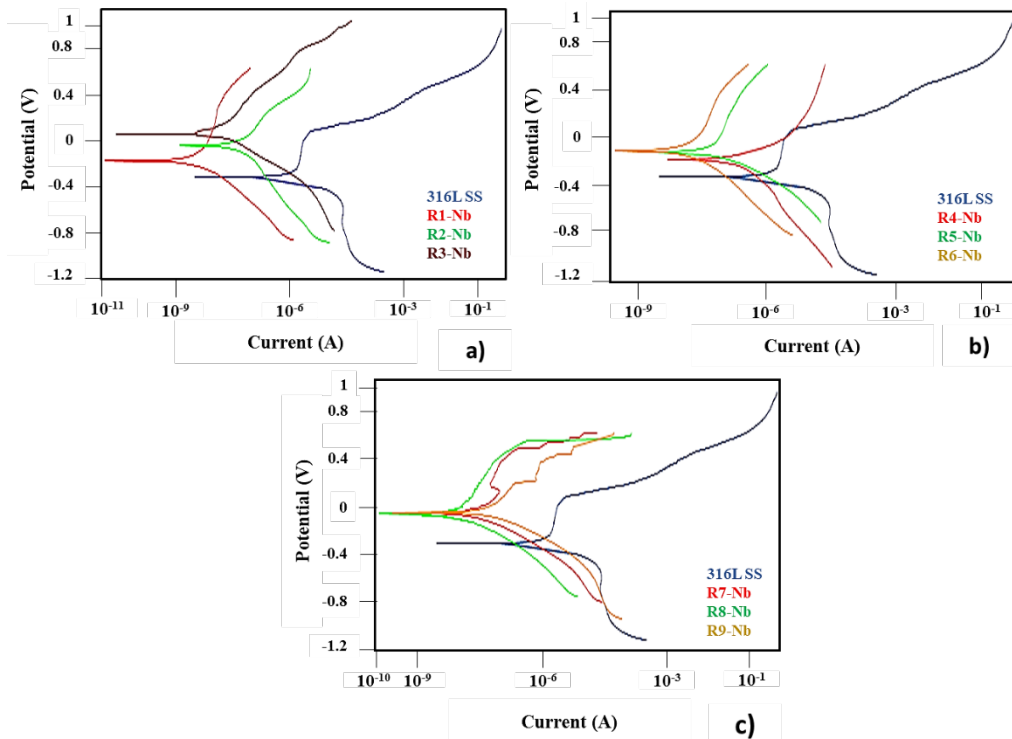
Fig. 10. Potentiodynamic curves of the substrate and CrYN:Nb thin films; **a)** R1-R3, **b)** R3-R6, **c)** R6-R9

All coated samples showed higher corrosion resistance than the uncoated substrate. Interpretations for corrosion samples were made according to the Icorr values. When the Tafel curves of Nb doped thin films are examined, the highest corrosion resistance is observed at R1, R3 and R8, respectively (Table 5). According to the same method, the lowest corrosion resistance was observed as Icorr 622.6 nA at R4. In addition, the increasing trend of Ecorr towards the positive direction indicates an increase in corrosion resistance.

Table 5. Corrosion parameters from the potentiodynamic polarization curves

	CrYN:Nb		CrYN:Ta	
	E_{corr} (mV)	I_{corr} (nA)	E_{corr} (mV)	I_{corr} (nA)
Substrate	-241	1826	-241	1826
R1	-174	4.4	-199	309.1
R2	-42	50.7	-33	17.8
R3	69	10.9	-199	446.6
R4	-196	622.6	14	5
R5	-103	37.2	-155	15.4
R6	-58	15	29	3.7
R7	-42	35	95	8.3
R8	-14	10.6	-103	60.9
R9	-51	33.3	-95	13.6
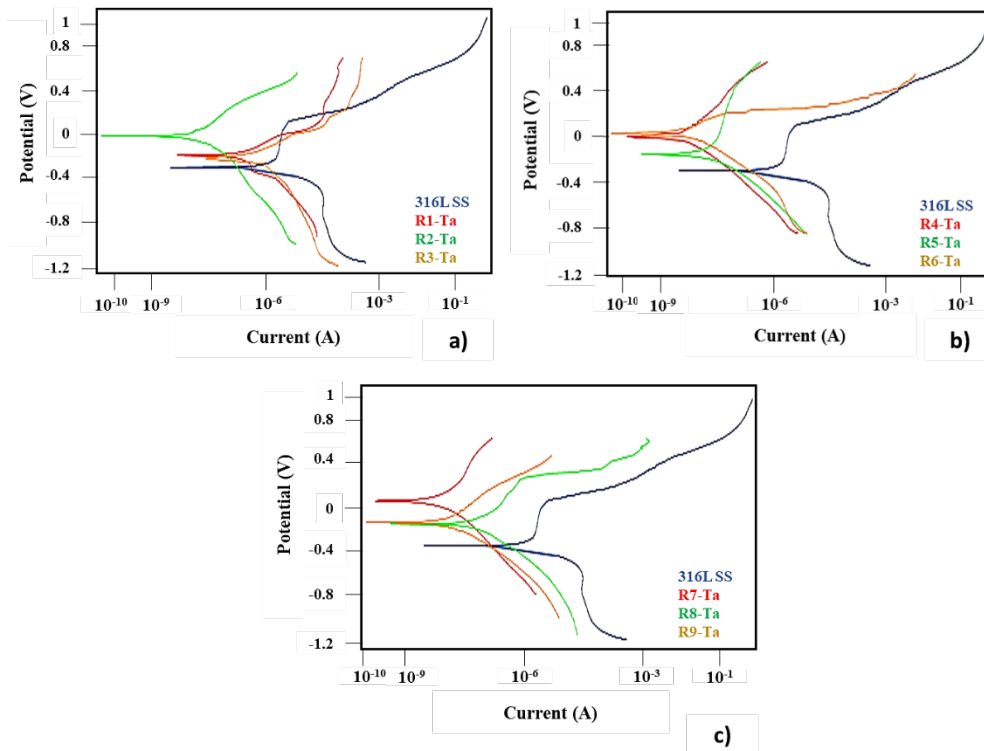
Fig. 11. Potentiodynamic curves of the substrate and CrYN:Ta thin films; **a)** R1-R3, **b)** R4-R6, **c)** R7-R9

According to the Tafel curves of the tantalum doped nitride films, the highest corrosion resistance was found at R6 with 3.7 nA, followed by R4 with 5 nA and R7 with 8.3 nA (Table 5). While the highest Icorr value was 446.6 nA for the tantalum doped thin films, this value was determined as 622.6 nA for the niobium doped films.

14
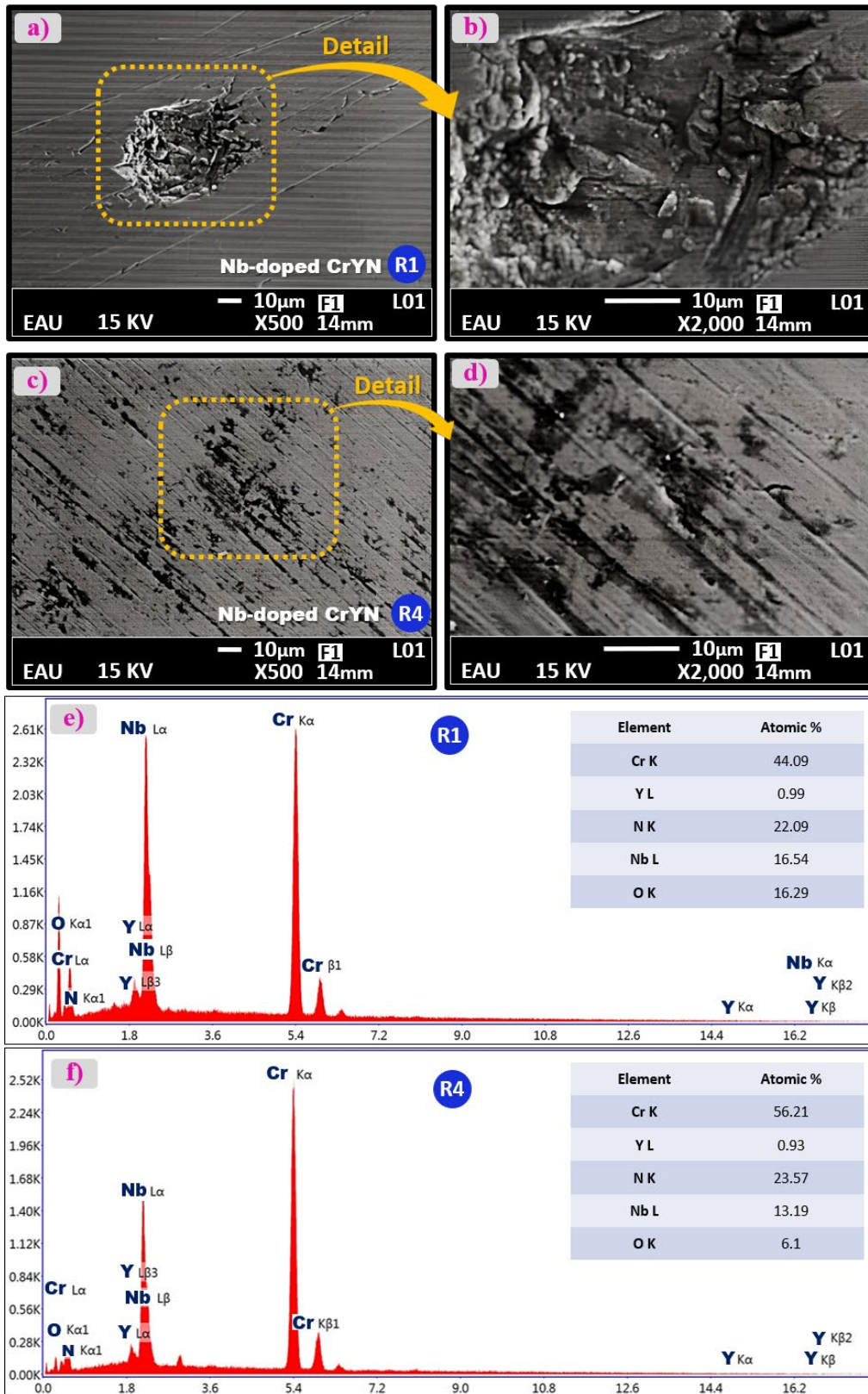
Fig. 12. SEM images and EDS analysis of CrYN:Nb thin films after corrosion, **a-b)** 500-2000 magnification image of the R1-Nb doped film, **c-d)** 500-2000 magnification image of the R4-Nb doped film, **e)** EDS analysis of the R1-Nb doped film after corrosion, **f)** EDS analysis of R4-Nb doped film after corrosion

SEM images of the samples showing the highest and lowest corrosion resistance after corrosion for CrYN:Nb/Ta films are given in Figure 12 and Figure 13. When R1, which shows the highest corrosion resistance in niobium doped films, is examined, it is observed that pitting corrosion occurs on the surface, while in R4, which shows the lowest corrosion resistance, uniform corrosion occurs on the entire surface.
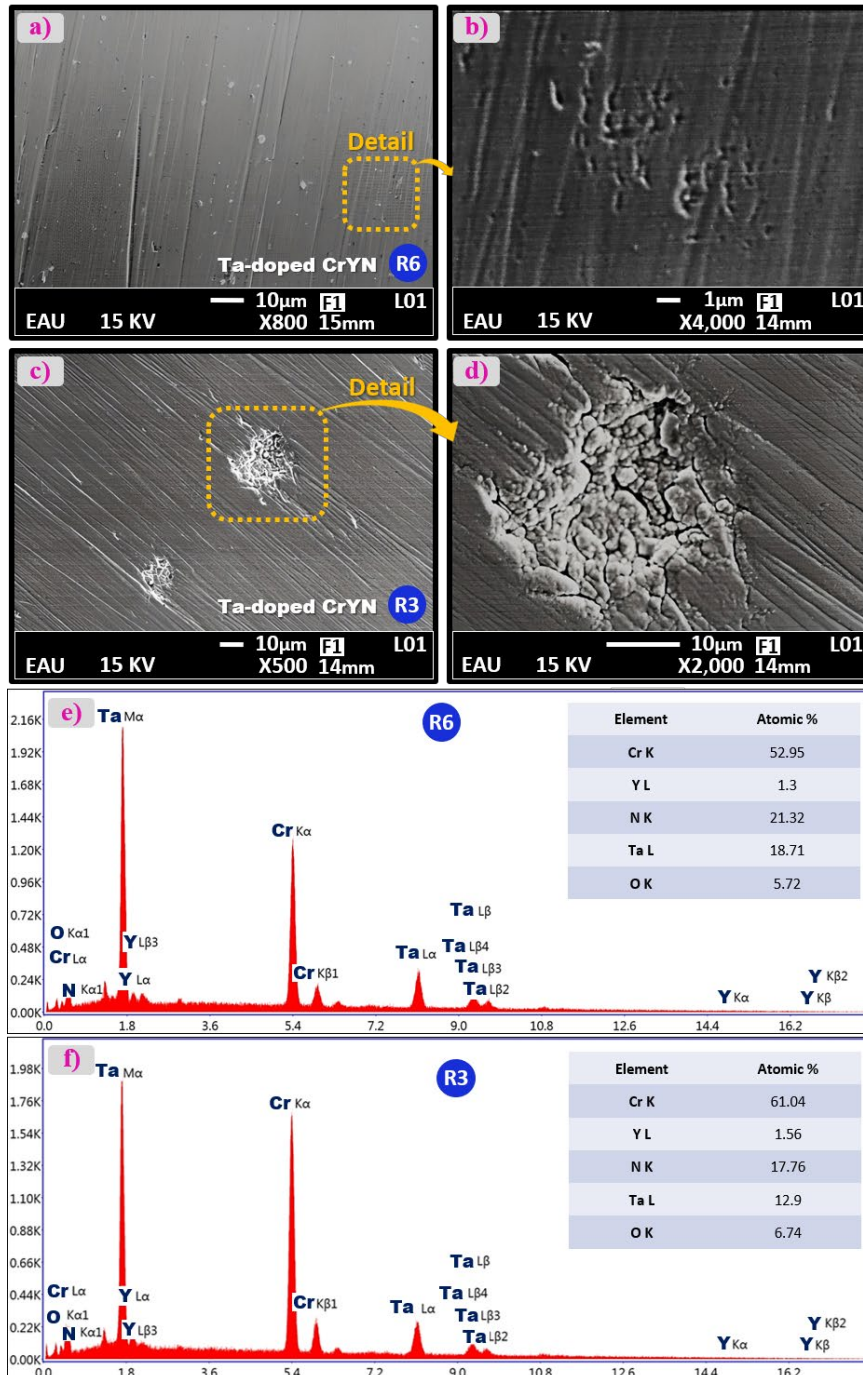
Fig. 13. SEM images and EDS analysis of CrYN:Ta thin films after corrosion, **a-b)** 800-4000 magnification image of the R6-Ta doped film, **c-d)** 500-2000 magnification image of the R3-Ta doped film, **e)** EDS analysis of the R6-Ta doped film after corrosion, **f)** EDS analysis of R3-Ta doped film after corrosion

The same kind of results were obtained for tantalum doped films. Pitting corrosion is present in R6, which shows the highest corrosion resistance, and in R3, which has the weakest corrosion resistance. After EDS analysis, the presence of oxygen was observed in all four samples. The atomic percentages of oxygen content for all thin films are as follows: R1 atomic 16.29%, R4 atomic 6.1%, R6 atomic 5.72%, R3 atomic 6.74% (Figure 12e-12f and Figure 13e-13f). It is known that both niobium and tantalum additives increase corrosion resistance [9, 16, 17], but it is clear that the corrosion resistance of tantalum is better than niobium in nitride-based films. Soleimani et al. conducted corrosion tests in artificial seawater environment for CrN/CrAlN thin films synthesized in PVD and the lowest Icorr value was observed as 0.057 µA. In a similar study, Man et al. reported the Icorr value of the coating with the highest corrosion resistance as 4.677 µA as a result of corrosion tests applied to CrYN thin films in NaCl solution [55, 56]. In our research, the Icorr values of the films with the highest corrosion resistance were found to be 0.0044 µA for niobium doped films and 0.0037 µA for tantalum doped films. This increase in corrosion resistance compared to other literature can be attributed to Nb and Ta doping. All coated samples showed higher corrosion resistance than the substrate in a saline water environment. CrYN:Nb/Ta films have a dense and highly homogeneous microstructure (Fig. 8), which improves corrosion resistance [55].

4. Conclusions

In this study, the mechanical, structural and chemical properties of Nb and Ta doped CrYN thin films grown on 316L SS substrate were investigated.

- ✓ XPS spectra were performed for CrYN:Nb/Ta thin films. For both thin films, scans were performed at Cr 2p, Y 3d and N 1s. In addition, the corresponding peaks were obtained at Nb 3d for niobium and Ta 4d for tantalum.

- ✓ Maximum nanohardness results for CrYN:Nb/Ta were determined as 21.4 GPa and 18.2 GPa, respectively. The most effective parameter affecting hardness in both films is the pulse frequency.

- ✓ When the XRD peaks of CrYN:Nb/Ta thin films and the substrate are analyzed, there are intense cubic CrN and Cr_2N peaks except for the main peaks coming from the substrate. NbN and TaN peaks were obtained in niobium and tantalum doped thin films, respectively. Yttrium is thought to be present in the structure as a substitutional atom of chromium.

✓ When the coating thicknesses and microstructure were examined, a dense and uniform structure was obtained in both composite thin films. The highest film thickness for niobium was observed in R3 at 2.80 μm and the thinnest film thickness was observed in R7 at 0.72 μm. Similar to the niobium doped film, the highest film thickness in the tantalum doped coating was found to be 2.26 μm at R3 (Pulse frequency 100 kHz, duty cycle 85%, deposition pressure 0.35 Pa, CrY target current 2A). The influence of the magnetron sputtered-pulsed dc power supply on the dense and uniform film structure cannot be ignored.

✓ The corrosion resistance of the coatings is quite high compared to the substrate. The lowest Icorr values for tantalum were found as 3.7 nA in R6, 5 nA in R4 and 8.3 nA in R7. Tafel curves show that the Icorr value of the substrate (316L SS) is 1826 nA, while the corrosion current values of Nb-doped CrYN thin films are much lower. The corrosion resistance of Nb-doped films was examined and it was found that even the film with the lowest corrosion resistance had approximately three times more resistance than the substrate. The lowest Icorr values for niobium were found to be 4.4 nA in R1, 10.6 nA in R8 and 10.9 nA in R3, respectively.

✓ In the SEM images after corrosion, the presence of pitting corrosion was observed similarly in both films. In niobium doped films, which are known to have lower corrosion resistance, the presence of both uniform and more intense and deep pitting corrosion was detected on the surface. When the positive effect of niobium and tantalum additives on corrosion is examined, it is seen that tantalum is a better corrosion barrier in these conditions.

Considering all these features, it seems that CrYN:Nb/Ta coatings are promising candidates to be used as a thermal barrier coating.

References

[1] H. Xu, H. Guo, Thermal barrier coatings, Woodhead Pub. Ltd. (2011) 1-69. https://www.sciencedirect.com/book/9781845696580/thermal-barrier-coatings

[2] H. Dong, G. J. Yang, C. X. Li, X. T. Luo, C. J. Li, Effect of TGO thickness on thermal cyclic lifetime and failure mode of plasma-sprayed TBCs, J. Am. Ceram. Soc. 97(4) (2014) 1226-1232. https://doi.org/10.1111/jace.12868

[3] W. Ma, H. Dong, Ceramic thermal barrier coating materials, In Thermal barrier coatings, (2011) 25-52. Woodhead publishing. https://doi.org/10.1533/9780857090829.1.25

[4] R. Vaßen, M. O. Jarligo, T. Steinke, D.E. Mack, D. Stöver, Overview on advanced thermal barrier coatings, Surf. Coat. Technol. 205(4) (2010) 938-942. https://doi.org/10.1016/j.surfcoat.2010.08.151

[5] O. Odabas, Y. Ozgurluk, D. Ozkan, G. Binal, I. Calis, A. C. Karaoglanli, Investigation of vermiculite infiltration effect on microstructural properties of thermal barrier coatings (TBCs) produced by electron beam physical vapor deposition method (EB-PVD), Surf. Coat. Technol. 443 (2022) 128645. https://doi.org/10.1016/j.surfcoat.2022.128645

[6] A. Avci, M. Karabaş, A.A. Eker, E. Akman, E., C. Aslan, Hot corrosion behavior of CYSZ thermal barrier coating with optimized laser surface modification, Ceram. Int. 49(19) (2023) 31396-31404. https://doi.org/10.1016/j.ceramint.2023.07.087

[7] L. Liu, S. Wang, B. Zhang, G. Jiang, H. Liu, J. Yang, W. Liu, Present status and prospects of nanostructured thermal barrier coatings and their performance improvement strategies: A review, J. Manuf. Process. 97 (2023)12-34. https://doi.org/10.1016/j.jmapro.2023.04.052

[8] M. Peters, C. Leyens, U. Schulz, W. A. Kaysser, EB-PVD thermal barrier coatings for aeroengines and gas turbines, Adv. Eng. Mater. 3(4) (2001) 193-204. https://onlinelibrary.wiley.com/doi/pdf/10.1002/1527-2648(200104)3:4%3C193::aid-adem193%3E3.0.co;2-u

[9] J. D. Osorio, A. Toro, J. P. Hernandez-Ortiz, Thermal barrier coatings for gas turbine applications: failure mechanisms and key microstructural features, Dyna, 79(176) (2012) 149-158. http://www.scielo.org.co/pdf/dyna/v79n176/v79n176a18.pdf

[10] N. P. Padture, M. Gell, E. H. Jordan, E. H, Thermal barrier coatings for gas-turbine engine applications, Science, 296(5566) (2002) 280-284. https://www.jstor.org/stable/pdf/3076507.pdf

[11] Z. Y. Wei, H. N. Cai, A. Tahir, W. W. Zhang, X. F. Li, Y. Zhang, Y., Y. Liu, Y, Stress states in plasma-sprayed thermal barrier coatings upon temperature cycling: Combined effects of creep, plastic deformation, and TGO growth, Ceram. Int. 45(16) (2019) 19829-19844. https://doi.org/10.1016/j.ceramint.2019.06.238

[12] X. Q. Cao, R. Vassen, D. Stöver, Ceramic materials for thermal barrier coatings, J. Eur. Ceram. Soc. 24(1) (2004) 1-10. https://doi.org/10.1016/S0955-2219(03)00129-8

[13] M. Karabaş, E. Bal, New Generation Thermal Barrier Coating Materials, Elec. J. Mach. Techn. 12 (1) (2015) 57-64. https://scholar.google.com.tr/scholar?hl=tr&as_sdt=0,5&cluster=191841685986193794

[14] A. Agüero, M. Juez-Lorenzo, P. E. Hovsepian, A. P. Ehiasarian, Y. P. Purandare, R. Muelas, Long-term behaviour of Nb and Cr nitrides nanostructured coatings under steam at 650 C, Mechanistic considerations, J. Alloys Compd. 739 (2018) 549-558. https://doi.org/10.1016/j.jallcom.2017.12.288

[15] P. E. Hovsepian, A. P. Ehiasarian, Y. P. Purandare, P. Mayr, K. G. Abstoss, M. M. Feijoo, J. P. Trujillo, Novel HIPIMS deposited nanostructured CrN/NbN coatings for environmental protection of steam turbine components, J. Alloys Compd. 746 (2018) 583-593. https://doi.org/10.1016/j.jallcom.2018.02.312

[16] G. V. Reddy, R. L. Krupakaran, H. Tarigonda, D. R. Reddy, N. G. Rasu, Energy balance and emission analysis on diesel engine using different thermal barrier coated pistons, Mater. Today : Proceedings. 43 (2021) 646-654. https://doi.org/10.1016/j.matpr.2020.12.424

[17] P. E. Hovsepian, A. P. Ehiasarian, Y. P. Purandare, B. Biswas, F. J. Pérez, M. I. Lasanta, A. Agüero, Performance of HIPIMS deposited CrN/NbN nanostructured coatings exposed to 650 C in pure steam environment, Mater. Chem. Phys. Materials. 179 (2016) 110-119. https://doi.org/10.1016/j.matchemphys.2016.05.017

[18] Y. C. Park, S.H. Lee, S. K. Kim, S. Lim, D. H. Jung, S. Y. Choi, D. H. Peck, Effects of CrN/Cr coating layer on durability of metal bipolar plates under a fuel recirculation system of direct methanol fuel cells, Int. J. Hydrog. Energy. 38(25) (2013) 10567-10576. https://doi.org/10.1016/j.ijhydene.2013.06.011

[19] S. Liu, Y. Yang, F. L. Ng, R. Ji, X. T. Zeng, Oxidation behaviour of CrAlYN coatings at elevated temperatures, Surf. Coat. Technol. 320 (2017) 357-361. https://doi.org/10.1016/j.surfcoat.2016.12.030

[20] P. E. Hovsepian, C. Reinhard, A. P. Ehiasarian, CrAlYN/CrN superlattice coatings deposited by the combined high power impulse magnetron sputtering/unbalanced magnetron sputtering technique, Surf. Coat. Technol. 201(7) (2006) 4105-4110. https://doi.org/10.1016/j.surfcoat.2006.08.027

[21] J. C. Walker, I. M. Ross, C. Reinhard, W. M. Rainforth, P. E. Hovsepian, High temperature tribological performance of CrAlYN/CrN nanoscale multilayer coatings deposited on γ-TiAl. Wear. 267(5-8) (2009) 965-975. https://doi.org/10.1016/j.wear.2009.01.039

[22] S. Domínguez-Meister, S. El Mrabet, R. Escobar-Galindo, A. Mariscal, M. J. De Haro, A. Justo, J. C. Sánchez-López, Role of Y in the oxidation resistance of CrAlYN coatings, Appl. Surf. Sci. 353 (2015) 504-511. https://doi.org/10.1016/j.apsusc.2015.06.099

[23] Z. T. Wu, Z. B. Qi, F. P. Zhu, B. Liu, Z. C. Wang, Influences of Y addition on mechanical properties and oxidation resistance of CrN coating, Phys. Procedia. 50 (2013) 150-155. https://doi.org/10.1016/j.phpro.2013.11.025

[24] Y.C. Chim, X.Z. Ding, X.T. Zeng, S. Zhang, Oxidation resistance of TiN, CrN, TiAlN and CrAlN coatings deposited by lateral rotating cathode arc, Thin Solid Films. 517 (2009) 4845–4849. https://doi.org/10.1016/J.TSF.2009.03.038.

[25] D. Wang, M. Hu, D. Jiang, Y. Fu, Q. Wang, J. Yang, J. Sun, L. Weng, The improved corrosion resistance of sputtered CrN thin films with Cr-ion bombardment layer by layer, Vacuum. 143 (2017) 329–335. https://doi.org/10.1016/j.vacuum.2017.06.040

[26] Z. Li, Y. Wang, X. Cheng, Z. Zeng, J. Li, X. Lu, L. Wang, Q. Xue, Continuously Growing Ultrathick CrN Coating to Achieve High Load-Bearing Capacity and Good Tribological Property, ACS Appl Mater Interfaces. 10 (2018) 2965–2975. https://pubs.acs.org/doi/pdf/10.1021/acsami.7b16426

[27] J. Zhang, Z. Li, Y. Wang, S. Zhou, Y. Wang, Z. Zeng, J. Li, A new method to improve the tribological performance of metal nitride coating: A case study for CrN coating, Vacuum. 173 (2020) 109158. https://doi.org/10.1016/j.vacuum.2019.109158

[28] S.B. Hung, C.F. Wang, Y. Y. Chen, J. W. Lee, C. L. Li, Thermal and corrosion properties of V-Nb-Mo-Ta-W and V-Nb-Mo-Ta-W-Cr-B high entropy alloy coatings, Surf. Coat. Technol. 375 (2019) 802-809. https://doi.org/10.1016/j.surfcoat.2019.07.079

[29] Z. T. Wu, Z. B. Qi, D. F. Zhang, B. B. Wei, Z. C. Wang, Evaluating the influence of adding Nb on microstructure, hardness and oxidation resistance of CrN coating, Surf. Coat. Technol. 289 (2016) 45-51. https://doi.org/10.1016/j.surfcoat.2016.01.047

[30] B. Trindade, W. Z. Li, F. Fernandes, A. Cavaleiro, Effect of Nb target power on the structure, mechanical properties, thermal stability and oxidation resistance of Cr–Al–Nb–N coatings, Surf. Coat. Technol. 285 (2016) 270-277. https://doi.org/10.1016/j.surfcoat.2015.12.002

[31] D. Wang, Y. Fu, M. Hu, D. Jiang, X. Gao, Q. Wang, L. Weng, Effect of Nb content on the microstructure and corrosion resistance of the sputtered Cr-Nb-N coatings, J. Alloys Compd. 740 (2018) 510-518. https://doi.org/10.1016/j.jallcom.2018.01.034

[32] J. Zhao, Y. Xu, Y, X. Ding, An in-depth understanding of the solvation effect of methanol on the anisotropy of electrochemical corrosion of Ta, Electrochim. Acta. 435, (2022). 141359. https://doi.org/10.1016/j.electacta.2022.141359

[33] M. L. Cedeno-Vente, J. Manriquez, G. C. Mondragón-Rodríguez, N. Camacho, A. E. Gomez-Ovalle, J. M. Gonzalez-Carmona, D. G. Espinosa-Arbelaez, Application of a transmission line model to evaluate the influence of structural defects on the corrosion behavior of arc-PVD CrN coatings, Ceram. Int. 47(15) (2021) 20885-20899. https://doi.org/10.1016/j.ceramint.2021.04.087

[34] S. H. A. N. Lei, Y. R. Zhang, Y. X. Wang, J. L. Li, X. Jiang, J. M. Chen, Corrosion and wear behaviors of PVD CrN and CrSiN coatings in seawater, Trans. Nonferrous Met. Soc. China. 26(1) (2016) 175-184. https://doi.org/10.1016/S1003-6326(16)64104-3

[35] Y. Vengesa, A. Fattah-alhosseini, H. Elmkhah, O. Imantalab, M. K. Keshavarz, Investigation of corrosion and tribological characteristics of annealed CrN/CrAlN

coatings deposited by CAE-PVD, Ceram. Int. 49(2) (2023) 3016-3029. https://doi.org/10.1016/j.ceramint.2022.09.286

[36] G. Bertrand, H. Mahdjoub, C. Meunier, A study of the corrosion behaviour and protective quality of sputtered chromium nitride coatings, Surf. Coat. Technol. 126(2-3) (2000) 199-209. https://doi.org/10.1016/S0257-8972(00)00527-2

[37] I. Efeoglu, G. Gülten, B. Yaylalı, Y. Totik, P. Kelly, J. Kulczyk-Malecka, Development of coatings for hostile environments, 2022.

[38] I. Bertóti, M. Mohai, P.H. Mayrhofer, C. Mitterer, Surface chemical changes induced by low-energy ion bombardment in chromium nitride layers, Surface and Interface Analysis. 34 (2002) 740–743. https://doi.org/10.1002/SIA.1401.

[39] M. Chen, S. Wang, J. Zhang, D. He, Y. Zhao, Synthesis of Stoichiometric and Bulk CrN through a Solid-State Ion-Exchange Reaction, Chemistry – A European Journal. 18 (2012) 15459–15463. https://doi.org/10.1002/CHEM.201202197.

[40] Z. Hui, X. Zuo, L. Ye, X. Wang, X. Zhu, Solution Processable CrN Thin Films: Thickness-Dependent Electrical Transport Properties, Materials 2020, Vol. 13, Page 417. 13 (2020) 417. https://doi.org/10.3390/MA13020417.

[41] X. Chen, Y. Du, Y. W. Chung, Commentary on using H/E and H^3/E^2 as proxies for fracture toughness of hard coatings, Thin Solid Films, 688 (2019) 137265. https://doi.org/10.1016/j.tsf.2019.04.040

[42] B. D. Beake, The influence of the H/E ratio on wear resistance of coating systems–Insights from small-scale testing, Surf. Coat. Technol. 442 (2022) 128272. https://doi.org/10.1016/j.surfcoat.2022.128272

[43] J. Blažek, J. Musil, P. Stupka, R. Čerstvý, J. Houška, Properties of nanocrystalline Al–Cu–O films reactively sputtered by DC pulse dual Magnetron, Applied Surface Science, 258(5) (2011) 1762-1767. https://doi.org/10.1016/j.apsusc.2011.10.039

[44] Z. T. Wu, Z. B. Qi, D. F. Zhang, B. B. Wei, Z. C. Wang, Evaluating the influence of adding Nb on microstructure, hardness and oxidation resistance of CrN coating, Surf. Coat. Technol. 289 (2016) 45-51. https://doi.org/10.1016/j.surfcoat.2016.01.047

[45] Y. I. Chen, Y. T. Lin, L. C. Chang, J. W. Lee, Preparation and annealing study of CrTaN coatings on WC-Co, Surf. Coat. Technol. *206*(7) (2011) 1640-1647. https://doi.org/10.1016/j.surfcoat.2011.06.012

[46] N. Schalk, M. Pohler, S. Hirn, V. T. Terziyska, P. Polcik, S. Kolozsvári, C. Czettl, Microstructure, mechanical properties and cutting performance of Cr1-yTayN single layer and Ti1-xAlxN/Cr1-yTayN multilayer coatings, Int. J. Refract. Hard Met. 71 (2018) 211-216. https://doi.org/10.1016/j.ijrmhm.2017.11.026

[47] A. Keleş, H. Çiçek, Ö. Baran, Y. Totik, İ. Efeoğlu, Determining the critical loads of V and Nb doped ternary TiN-based coatings deposited using CFUBMS on steels, Surf. Coat. Technol. 332 (2017) 168–173. https://doi.org/10.1016/j.surfcoat.2017.07.085

[48] S. Liu, B. De Ong, J. Guo, E. Liu, X. Zeng, X, Wear performance of Y-doped nanolayered CrN/AlN coatings, Surf. Coat. Technol. 367 (2019) 349-357. https://doi.org/10.1016/j.surfcoat.2019.02.092

[49] Z. B. Qi, Z. T. Wu, Z. C. Wang, Improved hardness and oxidation resistance for CrAlN hard coatings with Y addition by magnetron co-sputtering, Surf. Coat. Technol. 259 (2014) 146-151. https://doi.org/10.1016/j.surfcoat.2014.02.034

[50] M. T. Myandoab, CrAlYN/CrY Multilayer Composite Thin Film Synthesis: Structural-Mechanical-Tribological And Thermal Properties of Investigation. 2016, PhD Thesis. Institute of science. Ataturk university. https://tez.yok.gov.tr/UlusalTezMerkezi/tezDetay.jsp?id=y9uRDDYo9nldTmxEMvmqSQ&no=NLAGBOl6bic0vTM2WdfXUQ

[51] Y. Zhang, Q. Song, Z. Sun, Research on thin film thickness uniformity for deposition of rectangular planar sputtering target, Phys. Procedia. 32 (2012) 903-913. https://doi.org/10.1016/j.phpro.2012.03.655

[52] P. C. Huang, C. H. Huang, M. Y. Lin, C. Y. Chou, C. Y. Hsu, C. G. Kuo, The effect of sputtering parameters on the film properties of molybdenum back contact for CIGS solar cells, Int. J. Photoenergy. (2013). https://doi.org/10.1155/2013/390824

[53] W. Khan, Q. Wang, X. Jin, X, Effect of target composition and sputtering deposition parameters on the functional properties of nitrogenized Ag-permalloy flexible thin films deposited on polymer substrates, Materials. 11(3) (2018) 439. https://doi.org/10.3390/ma11030439

[54] P. J. Kelly, A. A. Onifade, Y. Zhou, G. C. Clarke, M. Audronis, J. W. Bradley, The influence of pulse frequency and duty on the deposition rate in pulsed magnetron sputtering, Plasma Process Polym. 4(3) (2007) 246-252. https://doi.org/10.1002/ppap.200600159

[55] M. Soleimani, A. Fattah-alhosseini, H. Elmkhah, K. Babaei, O. Imantalab, A comparison of tribological and corrosion behavior of PVD-deposited CrN/CrAlN and CrCN/CrAlCN nanostructured coatings, Ceram. Int. 49(3) (2023) 5029-5041. https://doi.org/10.1016/j.ceramint.2022.10.016

[56] M. Li, Y. Yu, C. Zou, C. Tian, Z. Wang, Y. Xiang, Wear and corrosion resistance of CrYN coating in artificial seawater, Metals. 13(2) (2023) 183. https://doi.org/10.3390/met13020183